

TERAHERTZ METAMATERIAL MODULATORS BASED ON ABSORPTION

H. Zhou¹, F. Ding^{1,2}, Y. Jin^{1,*}, and S. L. He^{1,2,3}

¹Centre for Optical and Electromagnetic Research, State Key Laboratory of Modern Optical Instrumentations, Zhejiang University, Hangzhou 310058, China

²ZJU-SCNU Joint Research Center of Photonics, South China Normal University, Guangzhou 510006, China

³Department of Electromagnetic Engineering, School of Electrical Engineering, Royal Institute of Technology, S-100 44 Stockholm, Sweden

Abstract—Metamaterial absorbers can perfectly absorb an incident wave in a narrow frequency band. In this paper, metamaterial absorbers are used to construct a terahertz modulator. By controlling the carrier density in the n -doped semiconductor spacer between a patterned metallic superstructure and a metallic ground with different applied voltage bias, the absorption varies sensitively, and the reflected wave amplitude acting as the modulated signal can be strongly modulated. Two types of modulators are investigated, one of which possesses an array of metallic crosses as the superstructure, and the other has a complementary superstructure. Compared with the former, the latter may give a better modulation performance.

1. INTRODUCTION

Metamaterials have produced many exotic effects such as negative refraction [1–4], zero refractive index [5–8], sub-wavelength imaging superlens [9], electromagnetic cloaking [10–13]. The novel properties of metamaterials come from the artificial atoms which can flexibly tailor the electric and magnetic response. The development of metamaterials is especially important for the terahertz (THz) frequency regime. Many natural materials inherently do not respond to THz radiation,

Received 13 June 2011, Accepted 15 August 2011, Scheduled 18 August 2011

* Corresponding author: Yi Jin (jinyi@coer.zju.edu.cn).

and many devices operating in this frequency range, such as sources, switches, modulators and detectors, are limited. Considerable efforts are underway to fill this THz gap in view of the potential applications of THz radiation. Metamaterials provide various possible ways for the THz area and have obtained a great of efforts, such as THz sensors, antennas, and chiral devices [14–16].

Recently, Landy et al. have proposed an innovative thin metal-dielectric composite called as a metamaterial absorber, in which the loss components of optical constants are utilized [17]. This is different from most other works which focus on the real parts of electric permittivity $\varepsilon(\omega)$ and magnetic permeability $\mu(\omega)$ and desire to get low loss. After that, some efforts have been made for metamaterial absorbers, such as polarization-insensitivity, omni-direction (wide-angle), and broad band [18–24].

Chen et al. have presented an efficient active THz metamaterial modulator [25], and Padilla et al. also found the efficient active THz metamaterial modulator works in another way nearly at the same time [26]. From then, a new research area has been created for active THz devices [27–30]. Although the metamaterial modulation is based on narrowband resonance, these devices can be engineered to operate at some specific frequencies. These modulators work by modulating the transmitted wave.

In this paper, THz metamaterial modulators based on absorber will be demonstrated for the first time to our knowledge, in which the reflected wave is modulated. By simply applying a tuning voltage bias, a depletion region with varied conductivity will be formed near the gap of the absorption structures to affect the strength of the resonance, and then different absorption of the incident wave can be effectively obtained.

2. METAMATERIAL ABSORBERS

Metamaterial absorbers are usually made of one patterned metallic film above one continuous metallic film with a dielectric spacer between them, and the two absorbers investigated in this paper are shown in Figs. 1(a) and 1(b), respectively. In Fig. 1(a), the patterned metallic film is composed of one array of discrete metallic crosses, and in Fig. 1(b), the patterned metallic film is the complementary structure of the former. Here, the used metal is copper with 0.2 μm -thickness. The array of metallic crosses is composition of two vertical cut-wire arrays. At the frequency of nearly perfect absorption, the relative effective permittivity and permeability of the metamaterial absorbers are nearly equal, and then nearly perfect impedance match is realized [31–33].

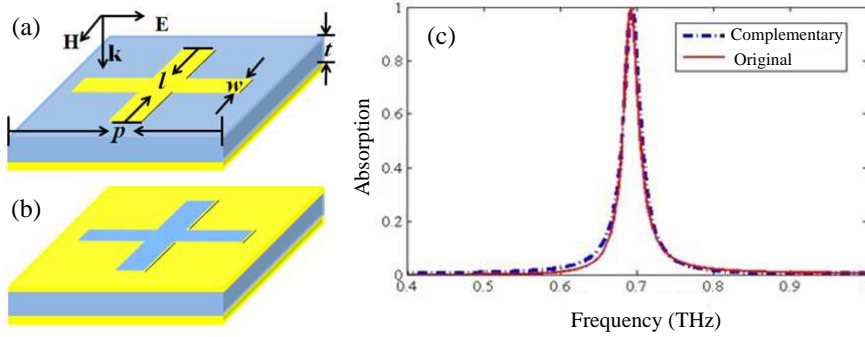


Figure 1. Geometric diagrams of the original absorber (a) and complementary absorber (b). (c) shows the absorption of two metamaterial absorbers. The solid curve (red) is for the original absorber, and the dashed one (blue) for the complementary absorber.

The incident wave can be strongly absorbed due to the large loss in the absorbers. Hereafter, the above two absorbers are called as original absorber and complementary absorber, respectively.

Now the absorption of the original and complementary absorbers is investigated by numerical simulation. For comparison, we would like to make the working frequencies of the two absorbers nearly the same (0.7 THz) at which the maximum absorption happens. The two absorbers have a period of $80 \mu\text{m}$. The arms of the crosses in the original absorber possess length $l = 64 \mu\text{m}$ and width $w = 6 \mu\text{m}$, while the cross gaps in the complementary absorber have $l = 74 \mu\text{m}$ and $w = 6 \mu\text{m}$. The dielectric spacer in the two structures is semi-insulating GaAs of conductivity $\sigma = 1 \text{ S/m}$, and the thickness is $t = 5 \mu\text{m}$ and $t = 7 \mu\text{m}$ for the original and complementary absorbers, respectively. The optimized absorption performance for normal incidence is shown in Fig. 1(c). The absorption can be up to about 99.9% in both absorbers.

Figure 2 shows the corresponding electric and magnetic field distributions when the two absorbers possess the maximum absorption. Charges of opposite signs accumulate at the two opposite ends of one arm in Fig. 2(a) for the original absorber, and at the opposite boundaries of one gap in Fig. 2(d) for the complementary absorber, which indicates the excitation of electric dipole resonance. These electric dipoles are greatly coupled with their own images which oscillate in anti-phase in the metallic substrate films [see Figs. 2(b) and 2(e)], and the coupling strength is mainly determined by the separation distance. Consequently, magnetic resonance is formed [34–36], which induces strong magnetic response [see Figs. 2(g) and 2(h)]. The electric

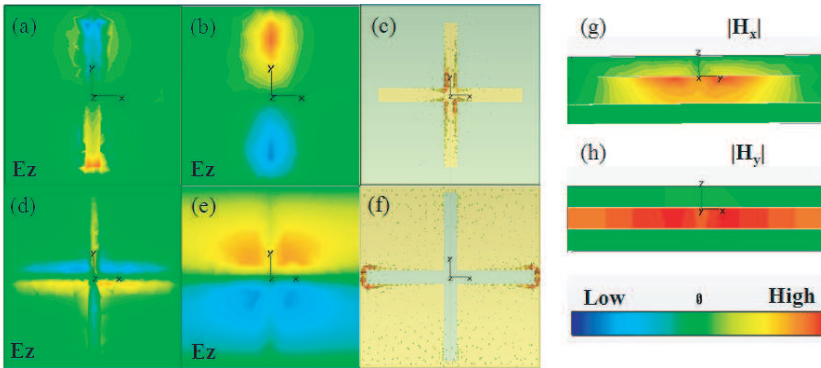


Figure 2. Field and current distributions when the original and complementary absorbers possess maximum absorption. (a)–(c) and (g) are for the original absorber, and (d)–(f) and (h) for the complementary one. (a) and (d) are the z -component electric field distributions on the top surfaces of the patterned metallic films, and (b) and (e) are for those on the surfaces of the homogeneous metallic substrates. (c) and (f) show the induced surface current distributions. (g) is the distribution of x -component magnetic magnitude in plane $x = 0$, and (h) for the distribution of y -component magnetic magnitude in plane $y = 40 \mu\text{m}$.

and magnetic resonance may make the absorbers impedance matched with free space, and an incident wave may be nearly perfectly absorbed by large loss.

3. THZ METAMATERIAL MODULATORS BASED ON ABSORPTION

From the above investigation, one can deduce that the absorption is determined by the electric and magnetic resonance. This means that one can tune the absorption by tuning the resonance strength. In the following, the original and complementary absorbers are applied for THz modulation by tuning the absorption. The structure configurations of the two modulators are illustrated in Fig. 3. $1 \mu\text{m}$ -thickness n -doped GaAs layer is grown on the semi-insulating GaAs layer of which the thickness is cut down by $1 \mu\text{m}$. The cells fabricated on the top of n -doped GaAs are connected together with thin metallic wires to serve as a metallic gate (Schottky), and a voltage bias is applied between the Schottky and Ohmic contacts.

The initial charge carrier density in the n -doped GaAs layer is

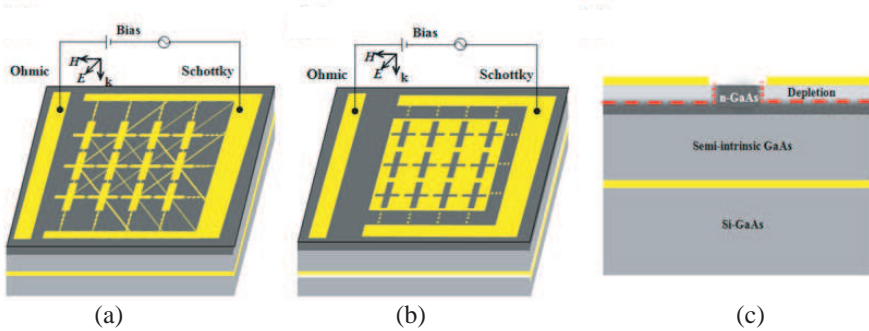


Figure 3. Modulators based on the cross absorber (a) and complementary absorber (b). (c) illustrates the depletion region near a gap, where the grey scale indicates the free charge carrier density. The gap may be the gap between neighboring metallic cross arms in (a), or a part of the gap crosses in (b).

proportional to the doping density. The charge carriers make the n -doped GaAs layer nearly conductive and make the metamaterial cells resonant weakly. The absorption of an absorber may be drastically degraded. When the voltage bias is applied and increased from zero, the charge carriers in the n -doped GaAs layer are gradually depleted gradually, and the n -doped GaAs layer is less conductive. Thus, the resonance of the absorbing cells is gradually enhanced, and the absorption is accordingly increased. The most important influence on the resonance strength comes from the part of the n -doped GaAs layer locating under the gaps which locate between neighboring metallic cross arms in the original modulator or act as a part of the gap crosses in the complementary modulator. This part is called n -doped GaAs gap hereafter. The above is the basic working mechanism of the suggested modulators based on absorption. The modulation depth is defined as the absorption difference when there is voltage bias or no.

When the voltage bias is applied, a depletion region in the n -doped GaAs layer with lower charge carrier density is formed. This can be verified by the comparison of the theoretical results from the semiconductor physic and the experimental results in Ref. [25]. The size of the depletion region depends on the applied voltage bias. If the applied voltage bias is not rather extreme, the part of the n -GaAs layer far away from the metallic crosses in the original modulator cannot be depleted, and the n -GaAs gaps in the complementary modulator are also not completely depleted since their width is rather larger than the thickness of the n -GaAs layer. For convenience, it is assumed that the depletion region is constant in size, in which the charge carrier density

depending on the voltage bias is uniform. Here in the simulation we suppose that in the original modulator, the depletion region of the n -doped GaAs crosses is directly under the metallic crosses, of which the arms are $2\ \mu\text{m}$ wider and longer than those of the metallic crosses, and in the complementary modulator, the n -doped GaAs crosses under the cross gaps excluding the $1\ \mu\text{m}$ -width sides are not depleted, and the other part of the n -doped GaAs layer belongs to the depletion region. In common tunable THz metamaterials, $1\ \mu\text{m}$ for the depletion width is reasonable when the bias voltage is large, which was also used in Ref. [30]. Although it is simplified in the present paper that the depletion region is of constant size, the obtained results can still well predict the main characteristics of a practical modulator based on absorption, and they are helpful for experimental realization.

If the whole n -doped GaAs layer is completely depleted, the absorption can be up to one. Now, because of the existence of the non-depletion region where high charge carrier density is residual, the maximum absorption is limited. That is to say, the modulation depth depends on the initial charge carrier density in the n -doped GaAs layer besides the voltage bias. This property is verified by numerical simulation shown in Fig. 4. The charge carrier density in n -doped GaAs is proportional to the conductivity and it is also proportional to the bias voltage. For convenience, the transverse axis in Fig. 4 is represented by the conductivity. One can find that rather large conductivity in the n -doped GaAs doesn't bring the largest modulate depth. For the best modulation performance, appropriate charge carrier density is needed. According to Fig. 4, the maximum modulation depth for the original modulator is about 0.45 when the conductivity of the n -doped GaAs is $\sigma_o = 1.0 \times 10^{2.4}\ \text{S/m}$, and it is about 0.7 for the complementary modulator when the conductivity is $\sigma_c = 1.0 \times 10^{4.4}\ \text{S/m}$. It is interesting that the complementary modulator can get much larger modulate depth than that of the original modulator. As we can see, when the voltage bias is not applied, the absorption of the two modulators is nearly the same (see the dashed lines in Fig. 4). When enough large voltage bias is applied to make the change carriers in the depletion region completely disappear, the absorption of the complementary modulator is much larger than that of the original modulator (see the solid curves in Fig. 4). This is caused by the size of the non-depletion region. As assumed in the above, the area of the non-depletion region in the original modulator is much larger than that in the complementary modulator.

Figure 5 shows the absorption spectrum as the increased voltage bias makes the conductivity in the depletion regions of the original and complementary modulators reduced gradually. The initial conductivity

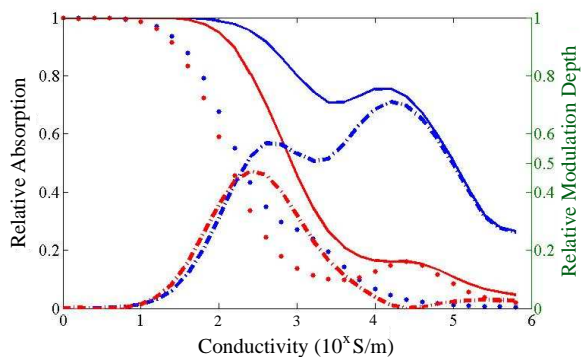


Figure 4. Absorption and modulation depth for different initial conductivity of the n -doped GaAs. The red curves are for the original modulator and the blue ones for the complementary modulator. The dashed curves represent the absorption when the voltage bias is not applied, and the solid ones represent the absorption when the applied voltage bias makes the change carriers completely disappear in the depletion region. The dot-dashed lines are for the modulation depth.

for the two modulators is σ_o and σ_c , respectively. In modulation, the absorption variation of the complementary modulator is more sensitive to the conductivity determined by the bias voltage than that of the original modulator. In Fig. 5(b), the red-shift of absorption peaks can be obviously found as the conductivity of the depletion region of the complementary modulator is increased. The relation between the absorption at a fixed frequency (0.71 THz and 0.67 THz for the original modulator and complementary modulator, respectively) and the conductivity of the depletion regions is shown in Fig. 5(c). The dashed lines represent the cut-off conductivities σ_d . This means that the conductivity of the n -doped GaAs can't be up over σ_d in the progress. It should be noted that as indicated in the above, even when the bias voltage is large to make the depletion region of the spacer possess low conductivity, the charge carriers in the other part of the spacer are not depleted, and the maximum absorption can not reach 100%.

Besides the modulation depth, modulation variation rate is also important for evaluating a modulator. The modulation rate at a fixed frequency is defined as

$$R = -\frac{dA}{d\sigma}. \tag{1}$$

The modulation rates of the two investigated modulators are shown in Fig. 6. The fixed frequency is f_o and the initial conductivity

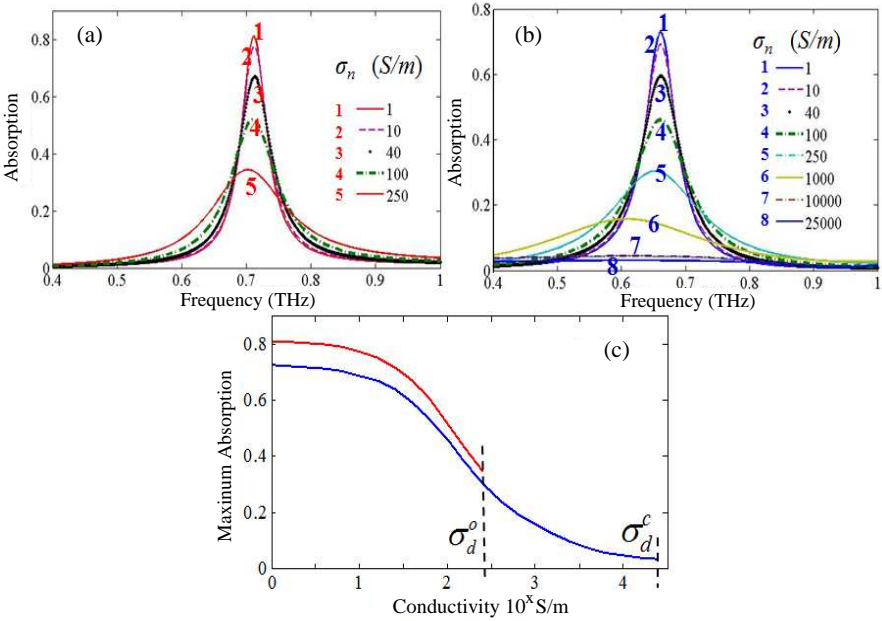


Figure 5. Absorption as the conductivity in the depletion region is varied by the voltage bias. (a) is for the original modulator, and (b) for the complementary modulator. The conductivity increases from curve 1 as the insert shows. (c) The relation of the absorption at the fixed frequency and the conductivity of the depletion region.

is σ_o for the original modulator, and for the complementary modulator they are f_c and σ_c , respectively. The instability might be caused by the sparse conductivity samples. In Fig. 6, one can see that the largest variation rate happens at a low conductivity. But as the difference of conductivity is small at the low conductivity, the difference of absorption at the fixed frequency is still small as shown in Fig. 5(c). And at the high conductivity, the rate is so small that the difference of absorption at the fixed frequency is small too.

In the above, the incident wave normally impinges on the modulators and only one polarization is investigated. In fact, the modulators are polarization-independent. Oliver Paul et al. have used the metallic crosses array for a polarization-independent active metamaterial for terahertz modulation [37]. Furthermore, the modulators are nearly omni-directional and the absorption performance is similar in a wide range of the incident angles, like the absorber in Ref. [24]. The above advantages have been verified by numerical simulation not shown here.

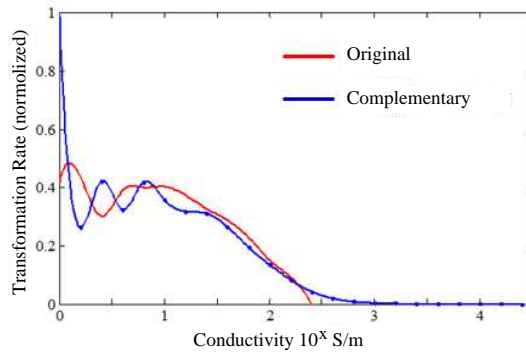


Figure 6. The normalized variation rate of the modulators.

4. CONCLUSION

The modulation performance of the original and complementary modulators based on the crosses array absorber and its complementary absorber has been demonstrated. The maximum modulation depths of the two modulators both depend on the conductivity of n -doped GaAs in the structures, and the modulation depth of the complementary can be much bigger than the original one as the gaps in them are different. The method used to calculate the optimal conductivity of the n -doped semiconductor layer might be helpful for the design of electrical modulators. Both of the two modulators behave much good modulation performances.

ACKNOWLEDGMENT

This work is partially supported by the National Natural Science Foundation (Nos. 60990322 and 60901039) of China. The partial support of AOARD is also gratefully acknowledged.

REFERENCES

1. Pendry, J. B., A. T. Holden, W. J. Stewart, and I. Youngs, "Extremely low frequency plasmons in metallic mesostructures," *Phys. Rev. Lett.*, Vol. 76, No. 25, 4773–4776, 1996.
2. Pendry, J. B., A. J. Holden, D. J. Robbins, and W. J. Stewart, "Magnetism from conductors, and enhanced non-linear phenomena," *IEEE Trans. Microw. Theory Tech.*, Vol. 47, 2075–2084, 1999.

3. Pendry, J. B., "A chiral route to negative refraction," *Science*, Vol. 306, 1353–1355, 2004.
4. Wu, Z., B. Q. Zeng, and S. Zhong, "A double-layer chiral metamaterial with negative index," *Journal of Electromagnetic Waves and Applications*, Vol. 24, No. 7, 983–992, 2010.
5. Enoch S., G. Tayeb, P. Sabouroux, N. Guérin, and P. Vincent, "A metamaterial for directive emission," *Phys. Rev. Lett.*, Vol. 89, No. 21, 213902, 2002.
6. Huang, X. Q., Y. Lai, Z. H. Hang, H. H. Zheng, and C. T. Chan, "Dirac cones induced by accidental degeneracy in photonic crystals and zero-refractive-index materials," *Nature Materials*, Vol. 10, 582–586, 2011.
7. Oraizi, H., A. Abdolali, and N. Vaseghi, "Application of double zero metamaterials as radar absorbing materials for the reduction of radar cross section," *Progress In Electromagnetics Research*, Vol. 101, 323–337, 2010.
8. Zhou, H., S. Qu, Z. Pei, Y. Yang, J. Zhang, J. Wang, H. Ma, C. Gu, X.-H. Wang, and Z. Xu, "A high-directive patch antenna based on all-dielectric near-zero-index metamaterial superstrates," *Journal of Electromagnetic Waves and Applications*, Vol. 24, No. 10, 1387–1396, 2010.
9. Pendry, J. B., "Negative refraction makes a perfect lens," *Phys. Rev. Lett.*, Vol. 85, 3966–3969, 2000.
10. Pendry, J. B., D. Schurig, and D. R. Smith, "Controlling electromagnetic fields," *Science*, Vol. 312, 1780–1782, 2006.
11. Chen, H. Y., C. T. Chan, and P. Sheng, "Transformation optics and metamaterials," *Nature Materials*, Vol. 9, 387–396, 2010.
12. Yu, G.-X., T.-J. Cui, W. Xiang, J. Xin, M. Yang, Q. Cheng, and Y. Hao, "Transformation of different kinds of electromagnetic waves using metamaterials," *Journal of Electromagnetic Waves and Applications*, Vol. 23, No. 5–6, 583–592, 2009.
13. Mei, Z. L., J. Bai, and T. J. Cui, "Illusion devices with quasi-conformal mapping," *Journal of Electromagnetic Waves and Applications*, Vol. 24, No. 17–18, 2561–2573, 2010.
14. O'Hara, J. F., R. Singh, et al., "Thin-film sensing with planar terahertz metamaterials: Sensitivity and limitations," *Opt. Express*, Vol. 16, No. 3, 1786–1795, 2008.
15. Singh, R., C. Rockstuhl, C. Menzel, T. P. Meyrath, M. He, H. Giessen, F. Lederer, and W. Zhang, "Spiral-type terahertz antennas and the manifestation of the Mushiake principle," *Opt. Express*, Vol. 17, No. 12, 9971–9980, 2009.

16. Singh, R., E. Plum, et al., "Terahertz metamaterial with asymmetric transmission," *Physical Review B*, Vol. 80, No. 15, 153104, 2009.
17. Landy, N. I., S. Sajuyigbe, J. J. Mock, D. R. Smith, and W. J. Padilla, "A perfect metamaterial absorber," *Phys. Rev. Lett.*, Vol. 100, 207402, 2008.
18. Landy, N. I., C. M. Bingham, T. Tyler, N. Jokerst, D. R. Smith, and W. J. Paddila, "Design, theory, and measurement of a polarization-insensitive absorber for terahertz imaging," *Phys. Rev. B*, Vol. 79, 125104, 2009.
19. Wang, J., S. Qu, Z. Fu, H. Ma, Y. Yang, X. Wu, Z. Xu, and M. Hao, "Three-dimensional metamaterial microwave absorbers composed of coplanar magnetic and electric resonators," *Progress In Electromagnetics Research Letters*, Vol. 7, 15–24, 2009.
20. Tao, H., C. M. Bingham, et al., "A dual band terahertz metamaterial absorber," *J. Phys. D: Appl. Phys.*, Vol. 43, 225102, 2010.
21. Zhu, B., Z. Wang, C. Huang, Y. Feng, J. Zhao, and T. Jiang, "Polarization insensitive metamaterial absorber with wide incident angle," *Progress In Electromagnetics Research*, Vol. 101, 231–239, 2010.
22. Gu C., S. Qu, Z. Pei, H. Zhou, J. Wang, B.-Q. Lin, Z. Xu, P. Bai, and W.-D. Peng, "A wide-band, polarization-insensitive and wide-angle terahertz metamaterial absorber," *Progress In Electromagnetics Research Letters*, Vol. 17, 171–179, 2010.
23. Huang, L. and H. Chen, "Multi-band and polarization insensitive metamaterial absorber," *Progress In Electromagnetics Research*, Vol. 113, 103–110, 2011.
24. Ye, Y. Q., Y. Jin, and S. L. He, "Omnidirectional, polarization-insensitive and broadband thin absorber in the terahertz regime," *J. Opt. Soc. Am. B*, Vol. 27, 498–504, 2010.
25. Chen, H. T., W. J. Padilla, J. M. O. Zide, A. C. Gossard, A. J. Taylor, and R. D. Averitt, "Active terahertz metamaterial devices," *Nature*, Vol. 444, 567–600, 2006.
26. Padilla, W. J., A. J. Taylor, et al., "Dynamical electric and magnetic metamaterial response at terahertz frequencies," *Physical Review Letters*, Vol. 96, No. 10, 107401, 2006.
27. Chen, H. T., W. J. Padilla, et al., "Ultrafast optical switching of terahertz metamaterials fabricated on ErAs/GaAs nanoisland superlattices," *Opt. Lett.*, Vol. 32, 1620–1622, 2007.

28. Chen, H. T., S. Palit, et al., "Hybrid metamaterials enable fast electrical modulation of freely propagating terahertz waves," *Appl. Phys. Lett.*, Vol. 93, 091117, 2008.
29. Chen, H. T., J. F. O'Hara, et al., "Experimental demonstration of frequency-agile terahertz metamaterials," *Nature Photon.*, Vol. 2, 295–298, 2008.
30. Chen, H. T., W. J. Padilla, et al., "A metamaterial solid-state terahertz phase modulator," *Nature Photon.*, Vol. 3, 148–151, 2009.
31. Chen, H. T., J. F. O'Hara, et al., "Complementary planar terahertz metamaterials," *Opt. Express*, Vol. 15, No. 3, 1084–1095, 2007.
32. Liu, X. L., T. Starr, A. F. Starr, and W. J. Padilla, "Infrared spatial and frequency selective metamaterial with near-unity absorbance," *Phys. Rev. Lett.*, Vol. 104, 207403, 2010.
33. Hao, J. M., L. Zhou, and M. Qiu, "Nearly total absorption of light and heat generation by plasmonic metamaterials," *Phys. Rev. B*, Vol. 83, 165107, 2011.
34. Liu, N., L. Fu, S. Kaiser, H. Schweizer, and H. Giessen, "Plasmonic building blocks for magnetic molecules in three-dimensional optical metamaterials," *Adv. Mater.*, Vol. 20, 3859–3865, 2008.
35. Li, T., H. Liu, F. M. Wang, Z. G. Dong, S. N. Zhu, and X. Zhang, "Coupling effect of magnetic polariton in perforated metal/dielectric layered metamaterials and its influence on negative refraction transmission," *Opt. Express*, Vol. 14, 11155–11163, 2006.
36. Liu, N., H. Guo, L. Fu, S. Kaiser, H. Schweizer, and H. Giessen, "Plasmon hybridization in stacked cut-wire metamaterials," *Adv. Mater.*, Vol. 19, 3628–3632, 2007.
37. Paul, O., C. Imhof, et al., "Polarization-independent active metamaterial for high-frequency terahertz modulation," *Opt. Express*, Vol. 17, No. 2, 819–827, 2009.